*"This is the accepted version of the following article: - Tailoring water stability of cellulose nanopaper by surface functionalization – Soft Matter 2018, 14, 7190, which has been published in final form at https://doi.org/10.1039/C8SM00433A.*

**Soft Matter**

ARTICLE

# Tailoring water stability of cellulose nanopaper by surface functionalization

Received 00th January 20xx,
Accepted 00th January 20xx

DOI: 10.1039/x0xx00000x

**www.rsc.org/**

Alessandra Operamolla,*[a] Stefano Casalini,[b,c] Dario Console,[a,d] Laura Capodieci,[e] Francesca Di Benedetto[e], Giuseppe Valerio Bianco[f] and Francesco Babudri[a]

Cellulose nanopaper (CNP) features appealing properties, including transparency, flatness, low thermal expansion coefficient and thermal stability, often outperforming conventional paper. However, free-standing crystalline cellulose films usually swell in water or upon moisture sorption, compromising part of their outstanding properties. This remains a major problem whenever working in water environment is required. Freestanding cellulose nanopaper is prepared by solution casting water suspensions of cellulose nanocrystals with avg width of 10 nm and avg aspect ratio of 28, isolated from Avicel by acid hydrolisis and extensively characterized by AFM and FE-SEM measurements and GPC detection of their degree of polymerization. We demonstrate by elemental analyses, FT-IR, Raman Spectroscopy, XRD measurements and water contact angle detection, that wet treatment with lauroyl chloride attains surface hydrophobization of nanopaper. The hydrophobized nanopaper, $C_{12}$-CNP, shows a more compact surface morphology than the starting CNP, as effect of the chemical functionalization, and presents enhanced resistance to water, as assessed by electrochemical permeation experiments. The new hydrophobized nanopaper is a promising substrate for thin film devices designed to work in a humid environment.

## Introduction

Natural materials are often composites comprising polymeric and/or ceramic components, with a complex hierarchical architecture that results from evolution and spontaneously forms in mild conditions.[1] Among them, cellulose represents the most abundant organic polymer on Earth and is easily accessible and cheap, as it is synthesized by plant cells and bacteria. Cellulose displays attractive potentialities for new technological applications due to its spontaneous assembly in crystalline fibrils.[2] Although early reports by Ramby[3] and by Battista et al.[4] clearly evidenced the possibility to perform acid digestion on cellulose, thereby isolating crystalline nanoparticles, only in the last decade nanocrystalline cellulose has attracted the interest of different industries and of the scientific community. This recent interest stems from its appealing features such as high tensile modulus, high specific surface area, biodegradability, biocompatibility and sustainability.[2,5,6] Cellulose nanocrystals (CNCs) are crystalline fibres featuring high aspect ratio with a diameter ranging from 5 to 50 nm and length between 100 and 500 nm.[7] CNCs are appealing in different scientific fields like the manufacturing of nanocomposites[8] and hydrogels,[9] drug delivery,[10] biocatalysts immobilization,[11] biosensors[12] etc. In particular, the intriguing perspective of using nanocellulose-based free-standing thin films, called cellulose nanopaper (CNP) for flexible electronics[13] has attracted much attention.[14] CNP represents an ideal substrate for electronics, whose actual challenges are not only flexibility, but also biocompatibility and a straightforward miniaturization. High throughput, cheapness, disposability, transparency,[15] biodegradability and biocompatibility are the pros that make CNP-based scaffolds extremely appealing. In addition, CNP-based thin films can display cholesteric chiral nematic ordering from which additional interesting optical properties arise;[16] further properties such as low thermal expansion coefficient, a wide compatibility with several thermal treatments, low surface roughness and good mechanical properties, yield even more versatile thin-films.[17] The CNP-based scaffolds meet the majority of specific requirements for printed electronics and biosensors, in fact scientific reports on the fabrication of electronic devices have appeared in the last years.[18,19,20,21,22,23,24] Fungal degradation of CNP for flexible transistors has been also demonstrated.[25] Even though a deep

[a] *Dipartimento di Chimica, Università degli Studi di Bari Aldo Moro, Via Orabona 4, I-70126 Bari, Italy. E-mail: alessandra.operamolla@uniba.it*
[b] *Università degli Studi di Modena e Reggio Emilia, Dipartimento di Scienze della Vita, via Campi 183, I-41100, Modena, Italy.*
[c] *Present address: University of Strasbourg, CNRS, ISIS UMR 7006, 8 Allée Gaspard Monge, F-67000 Strasbourg, France.*
[d] *Present address: DM Console srls, via Trieste 26, I-70043 Monopoli (BA), Italy.*
[e] *ENEA - Italian National Agency for New Technologies, Energy and Sustainable Economic Development, Laboratory for Functional Materials and Technologies for Sustainable Applications (SSPT-PROMAS-MATAS), S.S. 7 "Appia" km 706, I-72100 Brindisi (Br), Italy.*
[f] *Consiglio Nazionale delle Ricerche - Istituto di Nanotecnologia CNR-NANOTECH, via Orabona 4, I-70126 Bari (Ba), italy.*
† This paper was written through contribution of all authors.
Electronic Supplementary Information (ESI) available: Synthesis and purification details, full Raman-spectra, characterization of Avicel, wide area AFM and FE-SEM topographies, elemental analyses. See DOI: 10.1039/x0xx00000x

knowledge has been gained upon CNP, a rather overlooked issue is the water stability[26]. For instance, Zhou et al.[19a] have reported complete dissolution of the CNP-based substrate of a solar cell upon immersion in water for 30 minutes. Nanopaper is indeed a hydrophilic material due to the presence of surface free pending hydroxyl groups belonging to the $\beta$-D-glucopyranosidic rings composing the cellulose polymer chains. Water can hardly penetrate the cellulose crystalline structure,[27] which is very cohesive as effect of the cooperative and ordered interchain H-bond interactions, but it can easily leak in the cracks and spaces between the nanocrystals, yielding an overall swelling and a subsequent dissolution of the nanopaper in aqueous media. For the reasons above, this issue can be safely considered a hot-topic for the successful fabrication of electronic devices coupled to aqueous media, and only recent literature has started to consider this problem.[28] For this purpose, CNP should be turned in a water repellent material by chemical functionalization. In connection with our studies on new materials for organic electronics,[29] we prepare self-standing thin films of CNP by solution casting of an aqueous suspension of cellulose nanocrystals and tailor their surface with lauroyl ester groups. This functionalization is reached by a traditional alcohol esterification reaction and carried out dipping the nanopaper in dichloromethane in the presence of acyl chloride. We attain $C_{12}$-CNP that presents a functionalized surface, featuring a surface layer of pendant lauroyl ester groups, which are hydrophobic. We demonstrate that the reaction has little influence on the bulk crystallinity of the nanopaper, attaining very low cellulose degree of substitution by our wet treatment. The potential release of the acyl units as lauric acid in the environment may preserve nanopaper environmental harmlessness. The high stability against water over time of $C_{12}$-CNP with respect to the untreated nanopaper is successfully demonstrated by electrochemical investigation upon the water uptake into the CNP-based thin film.

## Results and discussion

### Preparation and characterization of cellulose nanocrystals (CNCs)

Nanocrystalline cellulose was isolated by acid hydrolysis of Avicel PH-101, a cotton linter-based commercial stationary phase for column chromatography. Avicel PH-101 is composed of microcrystalline cellulose whose particles have an average size of 45±5 µm, as judged from optical microscope analyses (see ESI, Figure S1). The acid hydrolysis was carried out in $H_2SO_4$: deionized water 1:1 v/v at 45°C for 80 minutes (see ESI for details on reaction yield and screening of reaction conditions). The reaction produced, after purification, a suspension of crystalline material in water at pH 7. The crystals were kept suspended by surface negative charges introduced by partial esterification of the primary alcohol functions on the C6 carbon of the glucopyranosidic units with sulfate groups.[30] Centrifugation allowed us to separate three different aliquots, whose characterization data are reported in the Table 1. The first one, termed "CNC4000", was isolated as the supernatant suspension upon centrifugation at 4000 rpm; the remaining two, termed "CNC3000" and "CNC2000" were separated from the residual material by performing centrifugation at 3000 and 2000 rpm, respectively. These aliquots (ESI, Figure S2) were composed of nanocellulose structures of different dimension. According to the average hydrodynamic diameter determined by dynamic light scattering (DLS) in aqueous solution, CNC4000 was the less polydisperse and it was composed by particles of diameter down to 82±15 nm; CNC3000 and CNC2000 displayed average diameter as high as 310±110 and 400±30 nm, respectively. The Table 1 summarizes properties of the three aliquots.

We measured average molecular weights and polydispersities of each CNC aliquot by gel permeation chromatography (GPC) in chloroform against polystyrene standards. We converted CNCs and Avicel into their hexanoyl derivatives by reaction with the corresponding acyl chloride in pyridine at 80°C, according to the Scheme 1. The esterification destroyed the crystalline aggregation by suppression of the cooperative inter- and intra-chain H-bonds, yielding a triester cellulose polymer soluble in dichloromethane and chloroform. This material was suitable for conventional GPC analysis in organic solvents.

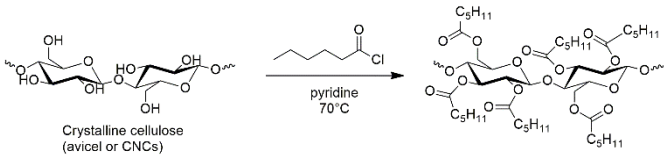


**Scheme 1.** Full esterification of cellulose with hexanoyl chloride.

**Table 1.** Characterization data of cellulose nanocrystals (CNCs)

| Aliquot | Centrifugation rate [rpm][a] | DLS average diameter [nm][b] | Average rod length (width) from AFM [nm][c] | Aspect ratio from AFM | Mn [Da][d] | Mw [Da][d] | PDI[d] (Mw/Mn) | DP[d] |
|---|---|---|---|---|---|---|---|---|
| CNC4000 | 4000 | 82±15 | 280±70 (10±2) | 28 | 63650 | 76410 | 1.20 | 140 |
| CNC3000 | 3000 | 310±110 | 400±60 (10±2) | 40 | 60830 | 82800 | 1.36 | 133 |
| CNC2000 | 2000 | 400±30 | N/A | N/A | 61940 | 96950 | 1.28 | 135 |
| Avicel PH-101 | -- | 45±5µm[f] | | | 69710 | 94100 | 1.35 | 153 |

[a] The centrifugation parameter defines the rate at which the nanocrystals fraction was isolated in the supernatant aqueous solution. [b] Estimated with the software LB-550. [c] Estimated from tapping AFM topographies acquired on nanocrystals deposited on glass from 0.01 % w/w solutions. [d] Average molecular weights, polydispersity index (PDI) and degree of polymerization (DP=Mn/MW; with MW=456Da,

 

molecular weight of the repetition unit of cellulose hexanoyl ester) were estimated from GPC measurements performed on the corresponding hexanoyl cellulose esters, synthesized according to the Scheme 2. [f] Average dimension of Avicel was judged from optical microscopy (see ESI for details).

Ioelovich[31] has shown that hydrolysis of Avicel produces nanocrystals with average degree of polymerization (DP) of 120-140 and that, if the DP lowers under this average value, the crystallinity is lost. In our experiments, Avicel displayed a number average molecular weight Mn of 68710 Da, while the CNC4000, CNC3000 and CNC2000 fractions showed a Mn value of 63650, 60830 and 61940 Da with a DP of 153 for Avicel and of 140, 133, and 135 for CNC4000, CNC3000 and CNC2000 aliquots, respectively. The data confirmed that DP was not compromised by the hydrolysis reaction, even in the presence of a consistent decrease in the aggregate dimension of crystalline cellulose, and this could be taken as an indirect proof of preserved crystallinity. Looking at the weight average molecular weight Mw, Avicel displayed a Mw of 94100 Da, while CNC4000, CNC3000 and CNC2000 fractions showed 76410, 82800 and 96950 Da Mw, respectively. Consequently, the less monodisperse cellulose was the CNC4000, with a polydispersity index (PDI) of 1.20. This was highly in accordance with the observed dispersity in the DLS hydrodynamic diameter, where an uncertainty of 11 nm was found over an average diameter of 82 nm. The other fractions were more polydisperse: the CNC3000 showed a PDI of 1.36, reflecting the very high uncertainty on the hydrodynamic diameter, while CNC2000 and Avicel had a PDI of 1.28 and 1.35, respectively.

Atomic force microscopy (AFM) was useful for a first morphological characterization of the nanocelluloses: topographies were acquired on solution cast thin films of the three aliquots. The AFM topographies (see Figures S3-4) certified the presence of rod-like crystals. The dimension of the rods was markedly different for each aliquot: the height distribution and the root mean square roughness increased in this fashion: CNC4000 < CNC3000 < CNC2000 (Please refer to ESI, Figure S4 for the histograms for each 10x10 $\mu m^2$ topography and Table S2 for the root mean square roughness values). These results clearly evidenced the increased dimension of nanocellulose rods in the CNC3000 and CNC2000 fractions. AFM allowed calculation of average length and width of CNC4000 and CNC3000 fractions. The same could not be performed on CNC2000 due to the highest roughness of the sample (see Figure S5, ESI, data for the sole CNC4000 fraction are shown). According to AFM, CNC4000 was composed of rods with length 280±70 nm, width 10±2 nm and aspect ratio 28, while CNC3000 was composed of rods with length 400±60 nm, width 10±2 nm and aspect ratio 40. The width, calculated by difference in heights and hence very close to real value, in each case suggested the presence of elementary nanofibrils that were cut by the acid digestion at different lengths. CNC4000, which revealed to be the less polydisperse aliquot according to DLS and GPC outcomes (with a PDI of 1.20), was deposited on silicon and further analyzed by FE-SEM technique (Figure 1), confirming the presence of rod-like nanocrystals and their dimension, in agreement with AFM.

**CNP deposition and hydrophobization**

Cellulose nanopaper can be prepared from CNCs suspensions in water by solution casting. As water evaporates, hydrogen bonds are established between nanocrystals, forming a network that detaches spontaneously as free-standing film. With the aim to produce the flattest nanopaper with limited voids, we casted CNC4000 solutions. As substrate, we used Kapton foils, that present excellent flatness. 1 mg/mL of glycerol was added to the solution as a plasticizer. The free-standing films were transparent, flat and flexible (see Figure S6). The average thickness was 32 $\mu m$.

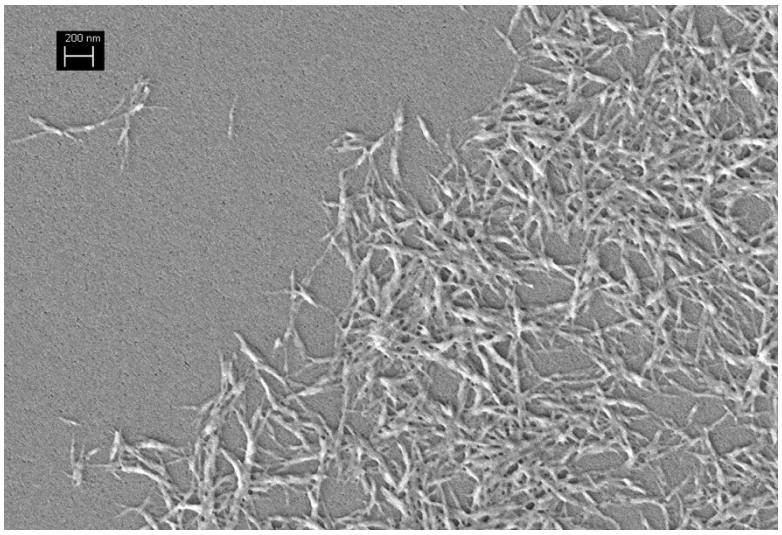


**Figure 1.** FE-SEM Micrograph of CNC4000 deposited by drop casting on silicon.

*"This is the accepted version of the following article: - Tailoring water stability of cellulose nanopaper by surface functionalization - Soft Matter 2018, 14, 7190, which has been published in final form at https://doi.org/10.1039/C8SM00433A.*

**Soft Matter**

ARTICLE

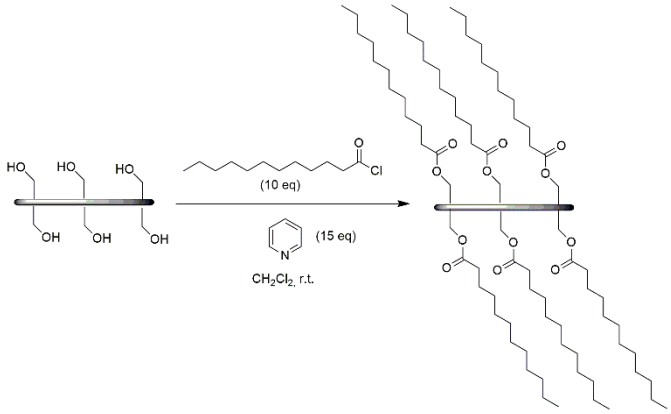


**Scheme 2.** Hydrophobization of nanopaper (CNP) with lauroyl chloride in dichloromethane and pyridine, producing $C_{12}$-CNP.

The surface functionalization was carried out by dipping the CNP thin film in a dichloromethane solution of lauroyl chloride and pyridine in a nitrogen filled glove-box at room temperature, according to Scheme 2. Pyridine had the role to convert the hydrochloric acid generated by the reaction in pyridinium chloride. The milder conditions of this reaction, with respect to the protocol presented in the Scheme 1, allowed us to control the functionalization of nanopaper, limiting the reaction to its surface, and to attain nanopaper with the desired hydrophobicity by tuning the relative amounts of acyl chloride and pyridine used and reaction times, as discussed below. Four different reaction conditions were tested, as reported in the table S3 in ESI. At the end of each experiment the success of the functionalization was detected by FT-IR analysis performed on the nanocellulose based films, recognizing the peak of the acyl C=O stretching at 1733 $cm^{-1}$. The use of high pyridine/cellulose molar ratios (entries 1-2) compromised the flexibility of nanopaper, resulting in brittle samples, even if shorter (1h) reaction times were adopted. We attributed this to possible cellulose phase transitions similar to those caused by interaction with alkali.[32] Consequently, we lowered the pyridine/cellulose molar ratios, that did not compromise the nanopaper flexibility, while keeping higher than 5 the molar ratio between acyl chloride and cellulose. We then chose the reaction conditions reported in entry 3 (the shortest reaction time with 10 equivalents of acyl chloride and 15 equivalents of pyridine). In order to demonstrate the correctness of our choice we fixed the reaction conditions of entry 3 and carried out chemical modifications experiment on CNP with lauroyl chloride changing the reaction time: we probed dipping times of 10, 30, 60 and 120 minutes. At the end of each experiment we washed the samples with dichloromethane and ethanol and carried out elemental analyses to detect an approximate degree of substitution of cellulose (DS) in dependence of the reaction time[33,34]. The results are collected in the table S4, reported in ESI. According to other authors, the degree of substitution (DS) of CNCs should be kept between 0.15 and 0.8 to ensure the involvement only of the skin of the nanocrystals and not the extension of the functionalization to their core.[35] We found that DS value increased from 0.011 for 10 minutes reaction time, to 0.023 for 30 minutes dipping and to 0.034 for 60 minutes dipping. The DS values were lower than the 0.15 limit value, but this is reasonable, because the functionalization involved only the surface of the nanopaper, while the elemental analyses are referred to the nanopaper bulk. Dipping CNP for 120 minutes yielded a DS of 0.018: the lower value could be reasonably ascribed to loss of some material due to too long reaction times. A possible extension of the reaction to the core of nanocrystals and solubilization of the surface cellulose triesters formed in the reaction medium may be the origin of material loss during the washing process. In conclusion, we chose 1 hour as total reaction time, that, according to elemental analyses, yielded a DS of 0.034 without apparent loss of material.

### Characterization of CNP and $C_{12}$-CNP

We then decided to perform an extensive characterization of the hydrophobized nanopaper($C_{12}$-CNP). The Figure 2a reports the FT-IR spectra that were acquired on CNP (black) and $C_{12}$-CNP (red). The hydrophobic CNP thin film spectrum did not show presence of adventitious pyridinium chloride salt formed during the reaction. The absence of adsorbed salt from the surface was confirmed by the absence of its characteristic and intense FT-IR bands at 2439, 1635, 1610, 1535, and 1485 $cm^{-1}$ and by elemental analyses that revealed no nitrogen content increase with the functionalization.[36] Moreover, the FT-IR spectrum of $C_{12}$-CNP showed the appearance of a distinct signal at 1733 $cm^{-1}$ in its FT-IR spectrum, which was ascribable to the C=O stretching of the ester group. The new band was partially overlapped to the band at 1647 $cm^{-1}$, attributed to crystallization water. The signal of free O-H single bonds stretching, centred at 3400 $cm^{-1}$, was persistent, suggesting a not complete functionalization of the cellulose backbone with ester groups. This supported the hypothesis that only the most reactive alcohol groups on the surface were transformed into lauroyl ester pendant groups by the wet treatment. In a parallel work[35a] the reaction of CNCs suspended in DMF at 90°C with acyl chlorides at different reaction time demonstrated progressive conversion of cellulose surface chains into a triester, with the reaction proceeding from the skin to the core of nanocrystals. This reactivity was hypothesized in our experiments too, and in order to understand this aspect, a cautious consideration of nanopaper bulk and surface crystallinity changes was taken into account.

Both spectra presented a typical absorption profile found for samples mainly composed of cellulose I (crystalline form mainly composing Avicel). As early reported by Nelson and O'Connor[37], the intensity of the absorption band at ca. 900 $cm^{-1}$ in the FT-IR spectrum increases with either a decrease in the crystallinity of the cellulose sample or a change in the crystal lattice from cellulose I to cellulose II or other allomorphs. Since our FT-IR spectra showed an increase in the mentioned band after hydrophobization, we carried out a deeper spectroscopic investigation on the effects of the dipping reaction to better understand the possible phase changes along with the cellulose hydrophobization.

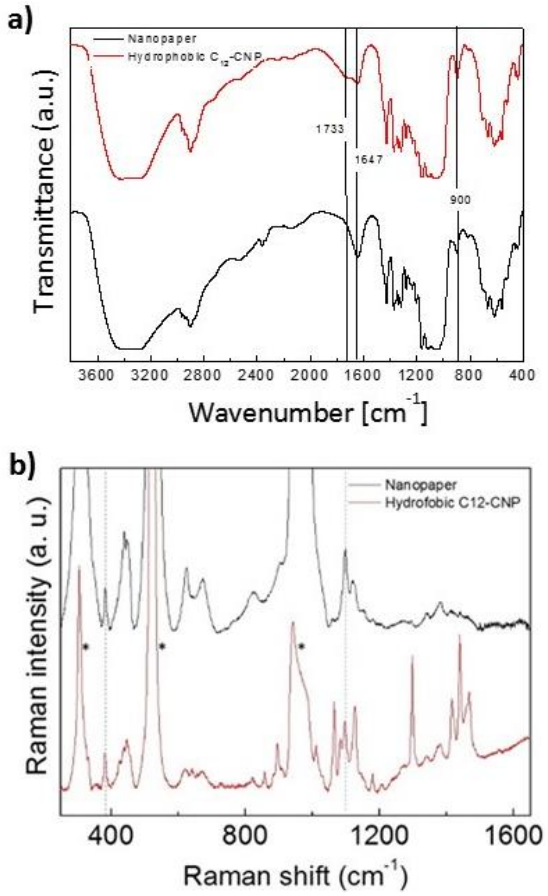


**Figure 2.** a) FT-IR spectra of nanopaper (black) and hydrophobic $C_{12}$-nanopaper (red) films. Vertical lines indicate signals centered at 1733, 1647 and 900 $cm^{-1}$. b) Raman spectra of nanopaper (black) and hydrophobic $C_{12}$-CNP (red) deposited on c-Si substrates. Dashed lines indicate, respectively, the cellulose Raman peaks at 380 $cm^{-1}$ and 1096 $cm^{-1}$. Raman features related to Silicon substrate modes have been labelled by *.

The Raman spectra of nanopaper (black) and hydrophobic $C_{12}$-CNP (red) are shown in Figure 2b. The successful nanopaper functionalization was attested by the appearance of new Raman modes in the red spectrum. Raman spectra of cellulose are very sensitive to differences in conformation and structural order, which can affect intensity, bandwidth and position of spectral features. In a comparative XRD/Raman investigation, Agarwal et al.[38] empirically demonstrated that the intensities of Raman peaks are differently affected by variations in the mass fraction of crystalline domains in cellulose materials. In particular, the relative intensity of the peak at 380 $cm^{-1}$, $I_{380}$, with respect to the peak at 1096 $cm^{-1}$, $I_{1096}$, was used in numerous cellulose studies as a measure of the degree of crystallinity.[38,39,40] We measured a value $I_{380}/I_{1096}$ around 1.1 from the Raman spectra of Avicel PH-101 (figure S7). This ratio decreased for the nanopaper Raman spectra (figure 2b). This agreed with the fairly lower polymerization degree found in CNC4000 with respect to Avicel. Conversely, Raman spectra in figure 2b revealed a higher value of the $I_{380}/I_{1096}$ ratio for the hydrophobic $C_{12}$-CNP, suggesting a structural reorganization of part of the cellulose composing the nanopaper after hydrophobization.

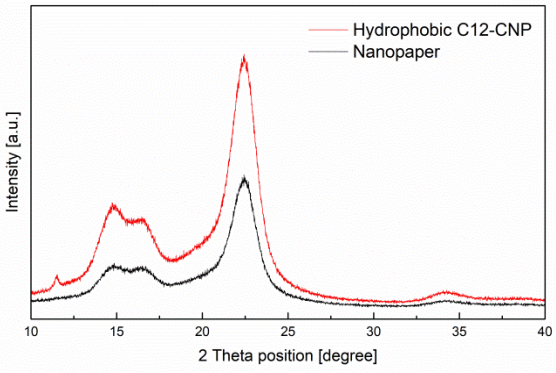


**Figure 3.** XRD pattern of nanopaper before (black) and after (red) the hydrophobization process.

A deeper analysis of the cellulose structural changes was performed by X-ray diffraction measurements operating under glancing incidence conditions. This particular configuration enables the identification of phases with increased surface sensitivity, limiting the X-ray penetration depth to the near surface zone of the CNP samples. Before the hydrophobization treatment the XRD pattern of CNP, black line in Figure 3, showed the characteristic spectrum of cellulose I/amorphous phase with diffraction peaks at 2θ angle of 14.7°, 16.4°, 22.4° and 34.4°, which could be assigned to the (1-10), (110), (200) and (004), respectively.[2] Conversely, the spectrum of hydrophobic $C_{12}$-CNP (red line in Figure 3), was characterized by more intense and better resolved Bragg's diffraction peaks without any shift in 2theta angle position. This suggested a lower amorphous character and a more ordered structure in $C_{12}$-CNP as a consequence of the reaction. Moreover, after the surface functionalization a low intensity diffraction peak at 11.5° appeared, which, coupled with an increase of the intensity in the range between 18° and 22°, could be ascribed to the presence of crystalline allomorphs of cellulose.[2] The line shape of the diffraction spectrum did not allow to discriminate between the presence of a single or a mixture of allomorphs, and further analyses, beyond the scope of this paper, will have to be performed in the future to get a deeper understanding of these aspects.

Further investigation on the surface of CNP and $C_{12}$-CNP was performed by atomic force microscopy in tapping mode and by water contact angle measurements (See Table 2 and Figure 4). The Figure 4 shows 2.5x2.5 $\mu m^2$ tapping mode AFM topographies of the pristine CNP surface with respect to the hydrophobic one. The former (Fig. 4a) showed the typical aggregation profile of CNCs nanocrystals, with rods intimately connected to each other by their longitudinal dimension. The pristine CNP film displayed a mean surface roughness of 7.7 ± 0.6 nm. The aggregation profile was still recognizable in the topography acquired after the functionalization based on

lauroyl chloride and pyridine, which demonstrated how the film texture was preserved even though a surface reorganization had occurred. Turning the hydrophilic CNP thin film into a hydrophobic one, the root mean square roughness decreased down to 5.0±0.7 nm. All these findings suggested surface functionalization and that lauroyl ester groups, possessing a linear and flexible aliphatic chain with a nominal length of approximately 1.6 nm, were homogeneously distributed over

**Table 2.** Characterization data of cellulose nanopaper (CNP) and hydrophobic nanopaper ($C_{12}$-CNP)

| | Water Contact Angle [°] | Root mean square roughness [nm][a] |
|---|---|---|
| CNP | 87±4 | 7.7±0.6 |
| $C_{12}$-CNP | 114±6 | 5.0±0.7 |

[a] Measured with the software XEI.

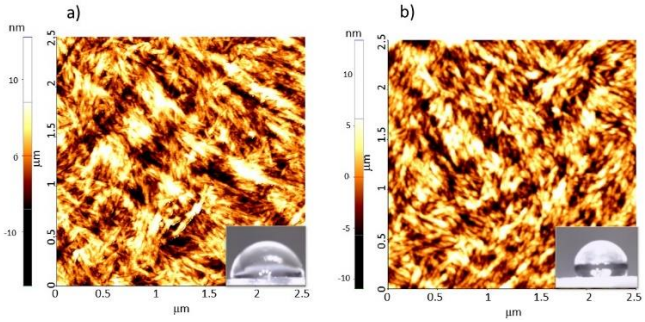


**Figure 4.** Tapping-mode 2.5x2.5 µm$^2$ AFM topographies of a) nanopaper from CNC4000 and b) nanopaper after hydrophobization with lauroyl chloride. Insets: water contact angle on the surface of the samples.

the surface of nanopaper, forming a layer potentially functioning as a barrier to water. This caused superficial fibres swelling, and the surface assumed a continuous film-like structure, with a corresponding decrease in roughness. FE-SEM micrographies on CNP and $C_{12}$-CNP, reported in Figure 5, were consistent with the picture given by AFM. The apparent increased compactness and more agglomerated structure observed in the micrograph recorded on $C_{12}$-CNP with respect to the hydrophilic CNP agreed with the decrease in surface roughness detected by AFM (compare also Figure S8, supplementary material with SEM micrographs acquired on larger areas).

Further information was offered by water contact angle measurements. In the case of bare CNP thin films, the water contact angle was equal to 87±4° (Table 2), but only for the first few seconds, since the water drop penetrated progressively into the nanocellulose film. This demonstrated the easy uptake of water into the pristine CNP thin films, whose primary effect is a swelling and an overall weakening of the film compactness. As mentioned in the introduction, this CNP limitation is still an open challenge into this field. A similar behaviour was observed for CNPs subjected to functionalization for 10, 30 and 40 minutes. Conversely, the contact angle of distilled water on the surface of hydrophobic $C_{12}$-CNP thin film was equal to 114±6°, which proved a dramatic change on the grade of wettability due to the successful functionalization. A further proof along this direction was the stability of the water drop onto the hydrophobic CNP. This allowed us to wash the $C_{12}$-CNP in ethanol and water at the end of the hydrophobization reaction.

**Water permeability tests**

The promising properties of $C_{12}$-CNP prompted us to investigate the water intake of these CNP-based thin films by means of electrochemical impedance spectroscopy (EIS). So far, the dramatic change of surface tension of the $C_{12}$-CNP thin film, recorded by contact angle measurement, did not furnish enough information about the water intake in the nanopaper bulk, nor allowed us to give a quantitative interpretation of the apparently increased surface hydrophobicity. For this purpose, we performed electrochemical measurements, which could provide a clear view about the water intake into our CNP samples with time and effectively prove the increased stability gained by $C_{12}$-CNP in water. EIS was previously successful for investigation of protective coatings against metal corrosion[41,42,43] and of biodegradation of enteric coatings.[44] In corrosion studies, by performing impedance measurements at low and high frequencies on metals covered by polymer protective coatings, it was possible to calculate their porosity.[45] The porosity was an expression of the number of defects per unit area: a defect-less metal protective coating would not be permeable to ions, oxygen and water. Conversely, defects would determine progressive penetration of the aqueous solution through the coating to the underlying metal. The presence (or absence) of thin channels of electrolyte running across the coating would appear as a coating bulk resistance $R_b$. A second parameter, the wetted area, was related to the fraction of the metal surface wetted by the aqueous solution. It could assume a different value from porosity when the aqueous solution contacting the electrode from a thin pore was spread

*"This is the accepted version of the following article: - Tailoring water stability of cellulose nanopaper by surface functionalization - Soft Matter 2018, 14, 7190, which has been published in final form at https://doi.org/10.1039/C8SM00433A.*

**Soft Matter**

ARTICLE

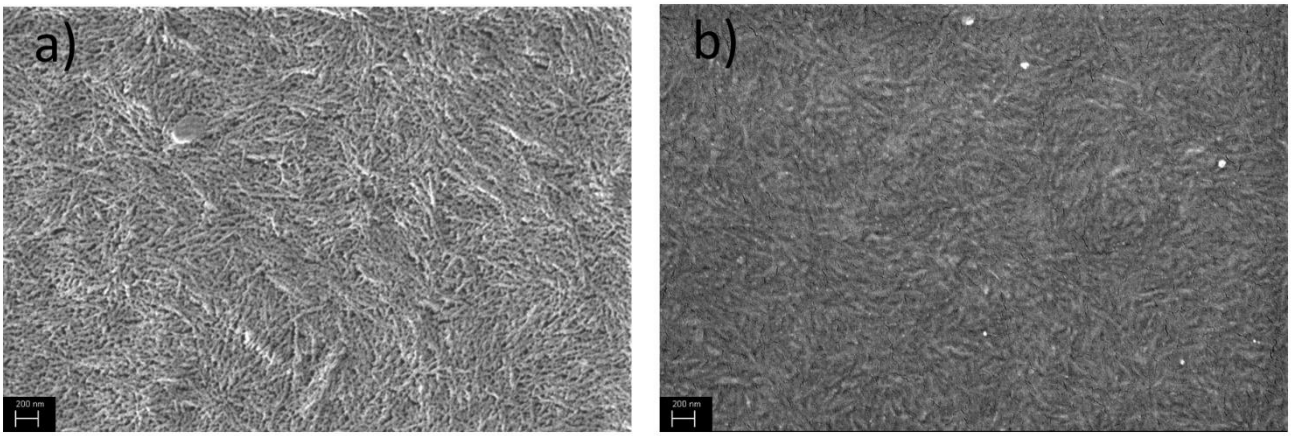


**Figure 5.** FE-SEM surface micrographs of a) CNP and b) $C_{12}$-CNP (scale bar 200 nm)

*"This is the accepted version of the following article: - Tailoring water stability of cellulose nanopaper by surface functionalization - Soft Matter 2018, 14, 7190, which has been published in final form at https://doi.org/10.1039/C8SM00433A.*

**Soft Matter**

ARTICLE

rapidly between the coating and the metal.

Accordingly, CNP and $C_{12}$-CNP thin films were placed onto a polycrystalline Au electrode to carry out impedance spectroscopy, by applying to the electrode a sinusoidal potential with a small amplitude (*i.e.* 10mV). Differently from those well-established corrosion tests, we performed measurements in a fully capacitive mode, namely avoiding any faradaic reactions (i.e. set potential fixed at 0V; for further details on the experimental setup see ESI Figure S9). The dramatic difference between CNP and $C_{12}$-CNP was here expressed by the necessity to fit the impedance data with two different equivalent circuits, termed circuit 1 for CNP and circuit 2 for $C_{12}$-CNP (reported in the Figure 6a and 6b, respectively). The two circuits presented the following electrochemical components: the resistance of the electrolyte solution ($R_S$), the above described resistance of the film bulk ($R_b$), the capacitance of the film bulk ($C_b$), a constant phase element that described the electrical double layer at the interface between the Au electrode and the CNP sample ($CPE_1$), a constant phase element that described an additional capacitive barrier detected solely in the $C_{12}$-CNP film ($CPE_2$).

The open porosity P was calculated from the ratio $R_{bt}/R_b$, in which $R_{bt}$ was the theoretical resistance of a layer of pure electrolyte featuring the same thickness as CNP, while $R_b$ was the nanopaper bulk resistance. The wetted area was calculated from the ratio $C_{dl}/C_{dl0}$, in which $C_{dl}$ was the double layer capacitance of the coated electrode and $C_{dl0}$ the double-layer capacitance of the bare electrode. As shown by the plot presented in the Figure 6c, the evolution over time of the dimensionless *P* parameters for pristine- (black squares) and $C_{12}$-CNP (red circles) showed a difference of almost two orders of magnitude in porosity value between the two different nanopaper samples recorded in more than two hours of electrochemical monitoring. Although the porosity of $C_{12}$-CNP was much lower than that of CNP, it was higher than found for the most insulating coatings: [45,46] dried and perfectly insulating coatings showed P values around $10^{-9}$÷$10^{-8}$, whereas partially wetted and/or degraded ones yielded higher P values, up to $10^{-4}$, closer to the values here found for $C_{12}$-CNP. We attributed this behaviour to the presence of crystallization water in our nanopaper (~8% by weight, see ESI - Table S4 for details), that was not removed by the treatments performed. However, the transition from $10^{-4}$ porosity for $C_{12}$-CNP to $10^{-2}$ for CNP yielded preservation of the former and complete dissolution of the latter in water. The kinetics of the process of dissolution of CNP in water was detected by monitoring the admittance value of $CPE_1$ with time. The corresponding plot, shown in the Figure 6d, provided a time constant equal to 14 minutes. This kinetics was representative for those samples that did not degrade almost instantaneously upon immersion in water. In circuit 2, the presence of two in-parallel branchs connecting $R_b$ or $C_b$ intrinsically certified no significant uptake of water, and the in-series $CPE_2$ could be directly correlated to the hydrophobic pendant groups on the nanopaper. The capacitive barrier value was 54(±12) $\mu F/cm^2$; in this case as well the difference from ideal capacitance values reported elsewhere for dry coatings was attributed to the crystallization water content of nanopaper.

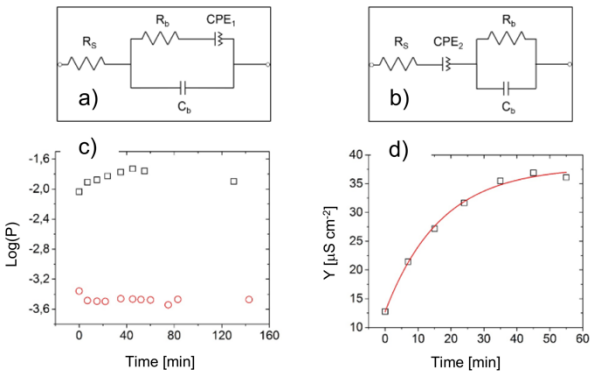


**Figure 6**. a) Equivalent circuit 1 (CNP) and b) circuit 2 ($C_{12}$-CNP); c) logarithm of the open porosity vs time plot. Black open squares and red open circles stand for the hydrophilic and hydrophobic CNP films, respectively; d) admittance Y vs time plot. The red line is the exponential fit.

## Experimental

### Materials and Methods

All reagents were purchased at the highest commercial quality and used without further purification. Avicel PH-101 was used as starting material for nanocrystalline cellulose isolation. Dry dichloromethane and pyridine were stored and dispensed in a nitrogen filled glove-box. Esterification reactions on nanocellulose were carried out under a nitrogen atmosphere in oven-dried glassware, using dry solvents. Sonication of water suspensions was carried out with a Bransson Sonifier 250. FTIR spectra were recorded on a Perkin–Elmer Spectrum BX spectrophotometer using dry KBr pellets when stated. Dynamic light scattering was carried out on a Particle Size Analyzer Horiba LB-550. A micrometer was used to determine the nanopaper thickness. Contact angle measurements were conducted using bi-distilled water. CHEM 3D Pro v. 12.0 drawing software was used to calculated the thoretical length of the dodecanoyl group on in vacuo optimized geometry.

**Hydrolysis of cellulose and nanocrystals isolation**

40 mL of deionized water were introduced in a 250 mL three necked round-bottom flask equipped with a water condenser and a mechanical stirrer. Then, the flask was cooled in an ice bath and 40 mL of concentrated $H_2SO_4$ were added. After that, 4g of Avicel PH-101 were added and the suspension was warmed to 50°C for 80 minutes. The system was cooled to room temperature and the mixture was transferred to polypropylene centrifugation tubes. Centrifugation at 4000 rpm was repeated replacing the supernatant solution with fresh deionized water until the pH was approximately 1. Then the precipitate was suspended in deionized water with the aid of a tip sonicator (power 2, duty cycle 60%, time 10 mins) and dialized against distilled water until neutrality using a cellulose nitrate membrane with a molecular weight cut-off of 12400 Da. The resulting suspension was transferred to polypropylene centrifugation tubes for the final fractionation as described in the ESI and Results and Discussion paragraph.

**Esterification of nanocrystalline cellulose with hexanoyl chloride**

4 mL of nanocrystals solution were transferred to a 25 mL two necked round bottom flask. Water was distilled through rotary evaporator, leaving a nanocellulose transparent film residue that was dried under vacuum. Then, the nanocellulose was weighed, and the flask was conditioned with nitrogen. 3 mL of dry pyridine were added, followed by esanoyl chloride (6 equivalents with respect to the amount of nanocellulose). The reaction mixture was heated at 80 °C for one night. The mixture turned from colourless to brown and the nanopaper film was completely consumed. The reaction mixture was cooled to room temperature and poured in a beaker containing 20 mL of HCl 3M and some ice. Then it was transferred to a 100 mL extracting funnel and extracted with dichloromethane (3 x 20 mL). The organic extracts were collected and washed with a 20 mL of a saturated solution of $NaHCO_3$ and a saturated solution of NaCl (2 x 20 mL). After that the organic extracts were dried over $Na_2SO_4$, filtered and the solvent was removed under reduced pressure. A brown solid was isolated. The crude material was purified by recrystallization from dichloromethane- methanol. A yellowish rubbery solid was isolated. FT-IR (KBr): $\nu$ 2960, 2855, 2360, 1740, 1460, 1261, 1162, 1055, 806 $cm^{-1}$.

**GPC molecular weights and polymerization degree determination**

GPC analysis was carried out at room temperature using a Malvern Viscotek TDA 305 equipped with a Tosoh Bioscience TSKgel G3000HHR column (7.8 mm i.d. × 30.0 cm l) using a refractive-index detector with chloroform as solvent. Calibration was performed using polystyrene standards. The polymers were dissolved in chloroform at 1mg/mL concentration and filtered prior to the measurement with 0.22 μm PTFE filters.

**Nanopaper preparation**

1 mg/mL of glycerol were added to a 1.8% w/w water suspension of cellulose nanocrystals. The suspension was sonicated for 20 minutes and it was poured on a Kapton foil and left to evaporate at 40°C in a common laboratory oven. At the end of the evaporation the nanopaper thin films detaches spontaneously from the substrate. A nanopaper with an average thickness of 32 μm and an area of approximately 5x5 $cm^2$ was obtained. For the following experiments the nanopaper was cut in 2x2 $cm^2$ or 1x1 $cm^2$ samples.

**Hydrophobization reaction on nanopaper**

The reaction was carried out in a nitrogen filled glove-box. A glass vessel was filled with 100 mL of anhydrous dichloromethane, 3.4 mL (42 mmol) of anhydrous pyridine and 6.5 mL (28 mmol) of lauroyl chloride. Then, a 455 mg sheet of nanopaper (2.8 mmol) was dipped in the mixture at room temperature for 1 hour. The reaction mixture turned from colorless to yellow. The nanopaper was removed, washed with 20 mL (4 x 5 mL) of clean dichloromethane, 20 mL of absolute ethanol and 20 mL of distilled water, and dried under vacuum. Finally, it was characterized by FT-IR spectroscopy, AFM, and contact angle measurement.

**Elemental analyses**

Elemental analyses were performed on a Carlo Erba EA 1108 CHNS Elemental analyzer. Sample preparation: the same nanopaper sample (prepared without glycerol additive) was cut into different pieces. Each sample was functionalized with pending lauroyl groups by dipping in the same conditions described above for: (i) 10 minutes, (ii) 30 minutes, (iii) 60 minutes and (iv) 120 minutes. At the end of the experiments the samples were washed with dichloromethane and ethanol and dried in vacuum.

**Raman Spectroscopy**

The Raman spectra of nanopaper were collected using a LabRAM HR Horiba-Jobin Yvon spectrometer with a 784 nm excitation laser source. The nanopaper samples were deposited on silicon by drop casting. The measurements were carried out under ambient conditions at a low laser power (1 mW) to avoid laser induced damage. The Raman band recorded from a silicon wafer at 520 $cm^{-1}$ was used to calibrate the spectrometer, and the accuracy of the spectral measurement was estimated to be around 1 $cm^{-1}$.

**Atomic Force Microscopy**

Atomic force microscopy topographies were taken using a Park XE-100 SPM system microscope. Images were acquired in the tapping mode using tips (Type PPP-NCHR) on a cantilever of 125 mm length, about 330 kHz resonance frequency, 42 N $m^{-1}$ nominal force constant and <10 nm guaranteed tip curvature radius. Surface areas were sampled with a scan rate of 1 Hz. Topographies were analysed using the software XEI (Park System Corporation, version 1.8.0).

**FE-SEM images**

The morphology of the surface of nanocrystalline cellulose was analyzed by FE-SEM, on a Field Emission Scanning Electron Microscope ZEISS Meriln® equipped with a GEMINI II® column and Beam-Booster, with acceleration voltages between 0.05 and 30 kV and 0.8nm as the best resolution, four optional detectors for SE and BSE, Charge Compensation and in situ Samples Cleaning system. Quartz 1x1 $cm^2$ glasses or silicon slabs with 1x1 $cm^2$ area were used as substrates for FE-SEM mesurements. All samples were allowed to dry overnight before analysis. For CNC4000 investigation, a solution 0.01% by weight of nanocrystals in water was drop cast on a silicon slab and after two minutes the solution residue was removed with filter paper. For nanopaper investigation, the pristine solution of CNC4000 was drop cast on quartz. One replicate was subjected to the hydrophobization reaction as described above.

**X-Ray diffraction measurements**

X-ray spectra were obtained on the cellulose nanopapers before and after hydrophobization treatment using a PANalytical EMPYREAN X-Ray diffractometer operating in the parallel beam geometry under glancing incidence conditions. The diffractometer was equipped with a copper radiation source (CuKα-radiation λ =0.154186 nm operating at 40kV\40 mA), x-ray mirror and post-sample collimator coupled with a flat graphite monochromator to ensure an intense monochromatic quasi-parallel incident beam for a good signal to noise ratio and an improved resolution. The data were recorded on samples of nanopaper of the same batch and thickness maintaining the incident angle ω (angle between the incident beam and sample surface) fixed at 1.0° and collecting the signal for 15 s per step with a 0.02° step size in the range between 10° and 40°.

**Electrochemical impedance spectroscopy characterization**

The impedance measurements were carried out in the following electrolytic solution: 0.1M NaCl and phosphate buffer 10mM set at pH 7.4. A home-built stage was used in order to guarantee a stable electrical connection between the working electrode (i.e. Au-coated quarz slide) and the counter electrode, which is a Pt wire (Ø 1mm). The NCP thin film was placed onto the golden-coated quartz slide. A further home-made system was built-up for confining the electrolytic solution as well as to fix the area wetted by the aqueous solution (i.e. 0.59 $cm^2$). The impedance measurements were performed by μ-AUTOLAB type III equipped with NOVA 1.10 software. The set potential was fixed at 0 V with an amplitude oscillation of 10 mV. The frequency rage spanned from $10^5$ Hz to $10^{-1}$ Hz with an acquisition time equal to 5 s. The electrochemical fits were performed by using the NOVA 1.10 software. According to our experimental setup, the $R_{bt}$ is equal to 0.42Ω. As well-defined in ref. 45, $R_{bt}$ is the theoretical resistance of a layer of electrolyte that occupies the same volume of our thin film during the electrochemical measurements.

## Conclusions

Performing acid hydrolysis of Avicel we were able to isolate in good yields water suspensions of cellulose nanocrystalline material. The nanocrystals were morphologically characterized by AFM and FE-SEM microscopies. The molecular weight of the cellulose polymer corresponding to the distinct crystalline structure was detected by gel permeation chromatography against polystyrene standards of the corresponding hexanoyl derivatives, finding polymerization degree (DP) values close to the one of the starting microcrystalline material.

The nanocrystals with the lowest dimension, but high aspect-ratio and low polidispersity, were used to prepare free-standing cellulose nanopaper (CNP) thin films. The cellulose nanopaper was hydrophobized by dipping in a dichloromethane solution of lauroyl chloride and pyridine and the preserved crystallinity and morphology and improved stability to water were demonstrated by AFM and FE-SEM microscopies, contact angle measurements, XRD spectroscopy and electrochemical water uptake experiments.

The hydrophobized nanopaper demonstrated in the present study displayed a very low degree of substitution, compatible with functionalization limited only to its surface. The treatment had an important impact on the water resistance properties of the nanopaper: the lauroyl functionalization layer yielded a nanopaper with significantly decreased porosity, as judged from electrochemical impedance spectroscopy. The open porosity electrochemical study highlighted the macroscopic bulk differences between the pristine CNP and the $C_{12}$-CNP films. The former was quickly degraded upon water exposure due to a fast water sorption. The latter was perfectly stable in water throughout the experiment timescale. This supported our claim that the stability of nanopaper in water had been significantly improved. We can conclude that $C_{12}$-CNP represents a very promising substrate for biodegradable and printed electronic devices and sensors.

## Acknowledgements

This work was financially supported by Regione Puglia, program FutureInResearch, project “SolarLeaf - Biodegradable organic solar cells supported on cellulose (Prot. F6YRA01)” and by Università degli Studi di Bari Aldo Moro. Mr Alberto Sacchetti is acknowledged for contact angle measurements, Dr. Danilo Vona for optical microscopy analysis on Avicel and Dr. Francesco Milano for DLS measurements.

## Notes and references

1 U. G. K. Wegst, H. Bai, E. Saiz, A. P. Tomsia and R. O Ritchie, *Nature Mater.*, 2015, **14**, 23.
2 *Handbook of Nanocellulose and Cellulose Nanocomposites*, H. Kargarzadeh, I. Ahmad, S. Thomas and A. Dufresne Eds., 2017, Wiley-VCH Verlag GmbH & Co. KGaA, Boschstr. 12, 69469, Weinheim, Germany.
3 B. G. Ranby, *Discussion Faraday Soc.* 1951, **11**, 158.
4 O. A. Battista, S. Coppick, J. A. Howsmon, F. F. Morehead and W. A. Sisson, *Ind. Eng. Chem.* 1956, **48**, 333.
5 Y. Habibi, L. A. Lucia and O. J. Rojas, *Chem. Rev.* 2010, **110**, 3479.
6 R. J. Moon, A. Martini, J. Simonsen and J. Youngblood, *Chem. Soc. Rev.* 2011, **40**, 3941.
7 *TAPPI Standards: Regulations and Style Guidelines, Standard Terms and Their Definition for Cellulose Nanomaterials*, W 13021.
8 a) M. Mariano, N. El Kissi and A. Dufresne, *J. Polym. Sci. B Polym. Phys.* 2014, **52**, 791; b) R. Xiong, Y. Han, Y. Wang, W. Zhang, X. Zhang, C.Lu, *Carbohydrate Polymers*, 2014, **113**, 264. c) Y. Yang, Z. Chen, X. Wu, X. Zhang, G. Yuan, *Cellulose*, 2018, **25**, 2547.
9 Z.-Y. Wu, H.-W. Liang, L.-F. Chen, B.-C. Hu and S.-H. Yu, *Acc. Chem. Res.* 2016, **49**, pp 96.
10 R. Sunasee, U. D. Hemraz, K. Ckless, *Expert Opin. Drug Del.*, 2016, **13**, 1243.
11 N. Grishkewich, N. Mohammed, J. Tang, K. C. Tam, *Curr. Opin. Coll. Inter. Sci.*, 2017, **29**, 32.
12 H. Golmohammadi, E. Morales-Narváez, T. Naghdi and Arben Merkoçl, *Chem. Mater.*, 2017, **29**, 5426.
13 a) D. Ha, Z. Fang, N. B. Zhitenev, Adv. Electron. Mater., 2018, 4, 1700593; b) M. Toivakka, J. Peltonen, R. Österbacka in Green Materials for Electronics, First Edition, Ch. 6, Eds M. Irimia-Vladu, E. D. Glowacki, N. S. Sariciftci, S. Bauer, 2018 Wiley-VCH Verlag GmbH & Co. KGaA. c) A. Operamolla, G. M. Farinola, Eur. J. Org. Chem. 2011, 3, 423; d) A. Operamolla, R. Ragni, F. Milano, R. R. Tangorra, A. Antonucci, A. Agostiano, M. Trotta, G. M. Farinola, *J. Mater. Chem. C*, 2015,3, 6471; e)

 

R. Ragni, A. Punzi, F. Babudri, G. M. Farinola, Eur. J. Org. Chem. 2018, doi: 10.1002/ejoc.201800657.
14 F. Hoeng, A. Denneulin and J. Bras, *Nanoscale*, 2016, **8**, 13131.
15 M. Nogi, S. Iwamoto, A. Norio Nakagaito and H. Yano, *Adv. Mater.*, 2009, **21**, 1595.
16 K. E. Shopsowitz, W. Y. Hamad and M. J. MacLachlan, *Angew. Chem. Int. Ed.*, 2011, **50**, 10991.
17 I. Gonzàlez, M. Alcalà, G. Chinga-Carrasco, F. Vilaseca, S. Boufi and P. Mutje, *Cellulose*, 2014, **21**, 2599.
18 a) H. Koga, M. Nogi, N. Komoda, T. T. Nge, T. Sugahara and K. Suganuma, *NPG Asia Mater.*, 2014, **6**, e93; b) L. Hu, G. Zheng, J. Yao, N. Liu, B. Weil, M. Eskilsson, E. Karabulut, Z. Ruan, S. Fan, J. T. Bloking, M. D. McGehee, L. Wågberg and Y. Cui, *Energy Environ. Sci.*, 2013, **6**, 513; c) Y. Song, Y. Jiang, L. Shi, S. Cao, X. Feng, M. Miao and J. Fang, *Nanoscale*, 2015, **7**, 13694.
19 a) Y. Zhou, C. Fuentes-Hernandez, T. M. Khan, J.-C. Liu, J. Hsu, J. W. Shim, A. Dindar, J. P. Youngblood, R. J. Moon and B. Kippelen, *Sci. Rep.*, 2013, **3**, 1536; b) M. Nogi, M. Karakawa, N. Komoda, H. Yagyu and T. T. Nge, *Sci. Rep.*, 2015, **5**, 17254; c) L. Hu, G. Zheng, J. Yao, N. Liu, B. Weil, M. Eskilsson, E. Karabulut, Z. Ruan, S. Fan, J. T. Bloking, M. D. McGehee, L. Wågberg, Y. Cui, Energy Environ. Sci. 2013, 6, 513; d) V. Costa, P. Pingel, S. Janietz, A. F. Nogueira, J. Appl. Polym. Sci. 2016, 133, 6; e) Zhou, Y., Khan, T.M., Liu, J.-C., Fuentes-Hernandez, C., Shim, J.W., Najafabadi, E., Youngblood, J.P., Moon, R.J., and Kippelen, B. (2014) Org. Electron., 15, 661–666; f) M.-H. Jung, N.-M. Park, S.-Y. Lee, Sol. Energy 2016, 139, 458.
20 a) Z. Fang, H. Zhu, W. Bao, C. Preston, Z. Liu, J. Dai, Y. Li and L. Hu, *Energy Environ. Sci.*, 2014, **7**, 3313; b) Y. Fujisaki, H. Koga, Y. Nakajima, M. Nakata, H. Tsuji, T. Yamamoto, T. Kurita, M. Nogi and N. Shimidzu, *Adv. Funct. Mater.*, 2014, **24**, 1657; c) D. Gaspar, S. N. Fernandes, A. G. de Oliveira, J. G. Fernandes, P. Grey, R. V Pontes, L. Pereira, R. Martins, M. H. Godinho and E. Fortunato, *Nanotechnology*, 2014, **25**, 094008; d) J. Huang, H. Zhu, Y. Chen, C. Preston, K. Rohrbach, J. Cumings and L. Hu, *ACS Nano*, 2013, **7**, 2106.
21 a) M. Nogi, N. Komoda, K. Otsuka and K. Suganuma, *Nanoscale*, 2013, **5**, 4395; b) T. Inui, H. Koga, M. Nogi, N. Komoda and K. Suganuma, Adv. Mater., 2015, **27**, 1112.
22 a) H. Zhu, Z. Xiao, D. Liu, Y. Li, N. J. Weadock, Z. Fang, J. Huang and L. Hu, *Energy Environ. Sci.*, 2013, **6**, 2105.
23 a) M.-C. Hsieh, C. Kim, M. Nogi and K. Suganuma, *Nanoscale*, 2013, **5**, 9289; b) M. Nogi and H. Yano, *Adv. Mater.*, 2008, **20**, 1849; c) Z. Wang, P. Tammela, P. Zhang, J. Huo, F. Ericson, M. Strømme and L. Nyholm, *Nanoscale*, 2014, **6**, 13068. 39.
24 K. Gao, Z. Shao, X. Wu, X. Wang, Y. Zhang, W. Wang, F. Wang, Nanoscale, 2013, 5, 5307.
25 J.-H. Seo, T.-H. Chang, J. Lee, R. Sabo, W. Zhou, Z. Cai, S. Gong and Z. Ma, *Appl. Phys. Lett.*, 2015, **106**, 262101.
26 a) H. Zhu, B. B. Narakathu, Z. Fang, A. Tausif Aijazi, M. Joyce, M. Atashbar and L. Hu, *Nanoscale*, 2014, **6**, 9110; b) A. G. Cunha, Q. Zhou, P. T. Larsson and L. A. Berglund, *Cellulose*, 2014, **21**, 2773; c) H. Sehaqui, T. Zimmermann and P. Tingaut, *Cellulose*, 2014, **21**, 367; d) Y. Su, Y. Zhao, H. Zhang, X. Feng, L. Shi and J. Fang, *J. Mater. Chem. C*, 2017, **5**, 573.
27 I. Sakurada, Y. Nukushima and T. Ito, *J. Polym. Sci.*, 1962, **57**, 651.
28 a) Q. Cheng, D. Ye, W. Yang, S. Zhang, H. Chen, C. Chang, L. Zhang, *ACS Sustainable Chem. Eng.*, 2018, **6**, 8040; b) S. Chen, Y. Song, F, Xu, *ACS Sustainable Chem. Eng.*, 2018, **6**, 5173; c) 32. P. Phanthong, G. Guan, S. Karnjanakom, X. Hao, Z. Wang, K. Kusakabed, A, Abudula, *RSC Adv.*, 2016, **6**, 13328.
29 a) A. Punzi, A. Operamolla, O. Hassan Omar, F. Brunetti, A. D. Scaccabarozzi, G. M. Farinola, N. Stingelin, *Chem. Mater.*, 2018, **30**, 2213; b) E. D. Głowacki, R. R. Tangorra, H. Coskun, D. Farka, A. Operamolla, Y. Kanbur, F. Milano, L. Giotta, G. M. Farinola, N. S. Sariciftci, J. Mater. Chem. C, 2015, 3, 6554; c) S. Casalini, M. Berto, F. Leonardi, A. Operamolla, C. A. Bortolotti, M. Borsari, W. F. Sun, R. Di Felice, S. Corni, C. Albonetti, O. Hassan Omar, G. M. Farinola, F. Biscarini, Langmuir, 2013, 29, 13198; d) V. Sgobba, G. Giancane, D. Cannoletta, A. Operamolla, O. Hassan Omar, G. M. Farinola, D. Guldi, L. Valli, ACS Appl. Mater. Interfaces 2014, 6, 1, 153; e) A. Operamolla, S. Colella, R. Musio, A. Loiudice, O. Hassan Omar, G. Melcarne, M. Mazzeo, G. Gigli, G. M. Farinola, F. Babudri, Sol. En. Mater. Sol. Cells, 2011, 95, 3490; f) O. Hassan Omar, F. Babudri, G. M. Farinola, F. Naso, A. Operamolla, A. Pedone, Tetrahedron, 2011, 67, 486.
30 R. H. Marchessault, F. F. Morehead and M. J. J. Koch, *Colloid. Sci.*, 1961, **16**, 327; J.-F. Revol, H. Bradford, J. Giasson, R. H. Marchessault and D. G. Gray, *Int. J. Biol. Macromol.*, 1992, **14**, 170.
31 M. Ioelovich, *Nanosci. Nanotec.*, 2012, **2**, 9.
32 A. Mittal, R. Katahira, M. E Himmel, D. K Johnson, *Biotechnology for Biofuels*, 2011, **4**, 41.
33 A. J. de Menezes, G. Siqueira, A. A. S. Curvelo, A. Dufresne, *Polymer*, 2009, **50**, 4552.
34 C. Vaca-Garcia, M. E. Borredon, A. Gaseta, *Cellulose*, 2001, **8**, 225.
35 a) M. Fumagalli, F. Sanchez, S. M. Boisseau, L. Heux, *Soft Matter*, 2013, **9**, 11309; b) M. Fumagalli, D. Ouhab, S. M. Boisseau, L. Heux, *Biomacromolecules*, 2013, **14**, 3246.
36 D. Cook, *Can. J. Chem.*, 1969, **39**, 2009.
37 M. L. Nelson, R. T. O'Connor, *J. Appl. Polym. Sci.*, 1964, **8**, 1325.
38 U. P. Agarwal, R. S. Reiner, S. A. Ralph, Cellulose, 2010, **17**, 721.
39 L. Berglund, M. Noël, Y. Aitomäki, T. Öman, K. Oksman, *Industrial Crops and Products*, 2016, **92**, 84.
40 U. P. Agarwal, "Raman Spectroscopy in the Analysis of Cellulose Nanomaterials", Chapter 4 in *Nanocelluloses: Their Preparation, Properties, and Applications*, U. P. Agarwal, R. H. Atalla and A. Isogai Eds., 2017, ACS Symposium Series, Vol. 1251, Washington, DC, American Chemical Society.
41 F. Mansfeld, *Corrosion*, 1981, **36**, 301.
42 E. Giusto, M. Donegà, A. C. Dumitru, G. Foschi, S. Casalini, M. Bianchi, T. Leonardi, A. Russo, L. G. Occhipinti, F. Biscarini, R. Garcia, S. Pluchino, *Adv. Biosys.*, **2017**, 1700021.
43 R.D. Armstrong, J. D. Wright, *Corrosion Science*, **1992**, *33*, 10, 1529.
44 C. J. McNeil, D. Athey, M. Ball, W. On No, S. Krause, R. D. Armstrong, J. D. Wright, K. Rawson, *Anal. Chem.*, **1995**, *67*, 3928.
45 R. D. Armstrong and J. D. Wright, *Electrochimica Acta*, 1993, **38**, 1779.
46 S. Krause, C. J. McNeil, R R.D. Armstrong, W. O. Ho, J. *Appl. Electrochem.*, **1997**, *27*, 291.